# Supporting Information for "Correlation between sea-level rise and aspects of future tropical cyclone activity in CMIP6 models"

Joseph W. Lockwood[1], Michael Oppenheimer[1,2,3], Ning Lin[4], Robert E.

Kopp[5,6], Gabriel A. Vecchi[1,3,7] and Avantika Gori[4]

[1]Department of Geoscience, Princeton University, NJ 08544, USA

[2]Princeton School of Public and International Affairs, Princeton University, Princeton, NJ 08544, USA

[3]High Meadows Environmental Institute, Princeton, NJ, USA

[4]Civil and Environmental Engineering, Princeton University, Princeton, NJ 08544, USA

[5]Institute of Earth, Ocean, and Atmospheric Sciences, Rutgers University, 71 Dudley Road, Suite 205, New Brunswick, NJ 08901,

USA

[6]Department of Earth and Planetary Sciences, Rutgers University, Piscataway, NJ, USA

[7]Atmospheric and Oceanic Sciences Program, Princeton University, Princeton, NJ, USA

## Contents of this file

1. Text S1

2. Figures S1 to S17

September 28, 2021, 2:53pm

## 1. Text S1

### 1.1. Sterodynamic sea-level

Most CMIP6 models utilized in this study are based on the Boussinesq approximation, conserving volume, not mass. As shown by Greatbatch (1994), such models are unable to capture the global mean thermosteric SLR associated with changes in the global mean density, with the bottom pressure also corrupted due to spurious mass sources required to conserve volume rather than mass. As some models used in this study do not have zostoga output, we calculate $h_\theta$ using potential temperature (thetao) referenced to the first year of each simulation (Griffies et al., 2016):

$$h_\theta = \left(\frac{V^0}{A}\right)\left(1 - \frac{\rho(\theta^\eta, S^0, p^0)}{\rho^0}\right) \tag{1}$$

where $V^0$ is the reference global volume of seawater and A is the area of the global ocean surface. The ocean density ($\rho$) in the numerator is computed as a function of the time evolving potential temperature, with salinity and pressure held constant at their reference value. Although halosteric sea-level change due to salinity changes, can be locally of the same order of magnitude as thermosteric, global-mean halosteric sea-level change is practically zero, and thus is often neglected. Spurious long-term drift is removed using at least 250 years of the models pre-industrial control simulation (piControl) (Gupta et al., 2013).

### 1.2. AIS SMB

Future Antarctic SMB is expected to increase in response to atmospheric warming as a result of enhanced snowfall, while runoff remains small (Palerme et al., 2017; Gorte et al., 2020). We construct anomalies in Antarctic SMB and its driving components, from the

finding in the high resolution regional atmospheric model MAR (Modele Atmospherique Regional) forced by an ensemble of CMIP6 models, that SMB changes are strongly correlated with the near-surface warming of the forcing ESMs around the AIS (Kittel et al., 2021):

$$\Delta SMB_{AIS} = TAS_{90-60°S} + 115.4 TAS_{90-60°S} - 11.1 \tag{2}$$

where $TAS_{90-60°S}$ is the surface temperature anomaly averaged between $90 - 60°S$.

Additionally, we estimate sea-level contribution from changes in Antarctic SMB from a parameterization based on regional climate output of different ESMs (Gregory & Huybrechts, 2006). This parameterization from Gregory and Huybrechts (2006) is based on the finding that net accumulation over the Antarctic ice-sheet increases with regional atmospheric warming:

$$\Delta SMB_{AIS} = AP\Delta T \tag{3}$$

Here, A is the time-mean snowfall accumulation during 1986-2010, equal to $1983 \pm 122$ Gt yr$^{-1}$ (Lenaerts et al., 2012). Factor P is the rate of increased accumulation per degree of regional atmospheric warming relative to this reference period, equal to 5.15% per degree, and $\Delta T$ is the anomaly in atmospheric temperature averaged over the Antarctic ice-sheet. Frieler et al. (2015) suggested an increase in accumulation linked to air temperature of 5-6% per degree Celsius, which is confirmed by SMB reconstructions from ice cores over the 20th century (Medley & Thomas, 2019). These two methods show good agreement (Fig. S17).

**References**

Frieler, K., Clark, P. U., He, F., Buizert, C., Reese, R., Ligtenberg, S. R. M., ... Levermann, A. (2015). Consistent evidence of increasing Antarctic accumulation with warming. , *5*(April), 1–5. doi: 10.1038/NCLIMATE2574

Fürst, J. J., Goelzer, H., & Huybrechts, P. (2015). Ice-dynamic projections of the greenland ice sheet in response to atmospheric and oceanic warming. *The Cryosphere*, *9*(3), 1039–1062. Retrieved from `https://tc.copernicus.org/articles/9/1039/2015/` doi: 10.5194/tc-9-1039-2015

Gorte, T., Lenaerts, J. T. M., & Medley, B. (2020). Scoring antarctic surface mass balance in climate models to refine future projections. *The Cryosphere*, *14*(12), 4719–4733. Retrieved from `https://tc.copernicus.org/articles/14/4719/2020/` doi: 10.5194/tc-14-4719-2020

Greatbatch, R. J. (1994). A note on the representation of steric sea level in models that conserve volume rather than mass. *Journal of Geophysical Research: Oceans*, *99*(C6), 12767-12771. Retrieved from `https://agupubs.onlinelibrary.wiley.com/doi/abs/10.1029/94JC00847` doi: https://doi.org/10.1029/94JC00847

Gregory, J., & Huybrechts, P. (2006). Ice-sheet contributions to future sea-level change. *Philosophical Transactions of the Royal Society A: Mathematical, Physical and Engineering Sciences*, *364*(1844), 1709-1732. doi: 10.1098/rsta.2006.1796

Griffies, S. M., Danabasoglu, G., Durack, P. J., Adcroft, A. J., Balaji, V., Böning, C. W., ... Yeager, S. G. (2016). OMIP contribution to CMIP6: Experimental and diagnostic protocol for the physical component of the Ocean Model Intercomparison Project. *Geoscientific Model Development*, *9*(9), 3231–3296. doi: 10.5194/gmd-9-3231-2016

Gupta, A. S., Jourdain, N. C., Brown, J. N., & Monselesan, D. (2013). Climate drift in the CMIP5 models. *Journal of Climate*, *26*(21), 8597–8615. doi: 10.1175/JCLI-D -12-00521.1

Kittel, C., Amory, C., Agosta, C., Jourdain, N. C., Hofer, S., Delhasse, A., . . . Fettweis, X. (2021). Diverging future surface mass balance between the Antarctic ice shelves and grounded ice sheet. , 1215–1236.

Lenaerts, J. T., Van Den Broeke, M. R., Van De Berg, W. J., Van Meijgaard, E., & Kuipers Munneke, P. (2012). A new, high-resolution surface mass balance map of Antarctica (1979-2010) based on regional atmospheric climate modeling. *Geophysical Research Letters*, *39*(4), 1–5. doi: 10.1029/2011GL050713

Medley, B., & Thomas, E. R. (2019). Increased snowfall over the Antarctic Ice Sheet mitigated twentieth-century sea-level rise. *Nature Climate Change*, *9*(January). Retrieved from `http://dx.doi.org/10.1038/s41558-018-0356-x` doi: 10.1038/ s41558-018-0356-x

Palerme, C., Genthon, C., Claud, C., Kay, J., Wood, N., & L'Ecuyer, T. (2017, 01). Evaluation of current and projected antarctic precipitation in cmip5 models. *Climate Dynamics*, *48*. doi: 10.1007/s00382-016-3071-1

Wang, C., Soden, B. J., Yang, W., & Vecchi, G. A. (2021). Compensation between cloud feedback and aerosol-cloud interaction in cmip6 models. *Geophysical Research Letters*, *48*(4), e2020GL091024. Retrieved from `https://agupubs.onlinelibrary .wiley.com/doi/abs/10.1029/2020GL091024` (e2020GL091024 2020GL091024) doi: https://doi.org/10.1029/2020GL091024

Zelinka, M. D., Myers, T. A., McCoy, D. T., Po-Chedley, S., Caldwell, P. M., Ceppi, P.,

. . . Taylor, K. E. (2020). Causes of higher climate sensitivity in cmip6 models. *Geophysical Research Letters*, *47*(1), e2019GL085782. Retrieved from `https://agupubs` `.onlinelibrary.wiley.com/doi/abs/10.1029/2019GL085782`    (e2019GL085782 10.1029/2019GL085782) doi: https://doi.org/10.1029/2019GL085782
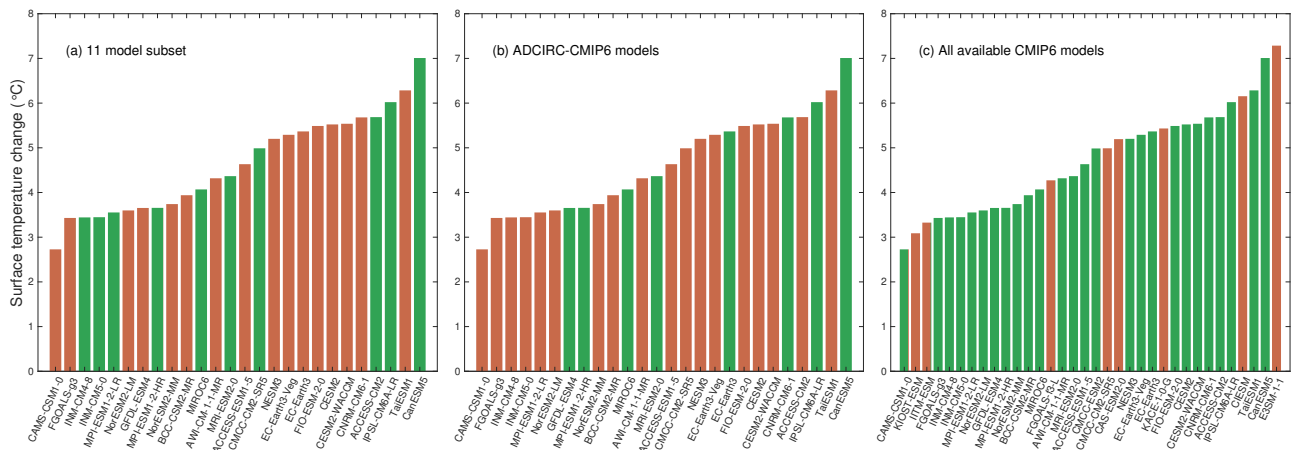
**Figure S1.** Projections of global mean temperature change (tas) change for (a) the 11 model subset, (b) for the models used in ADCIRC modeling and (c) all 34 CMIP6 models with available tas variable for the simulations and run used in this study. Green denotes models used in analysis.
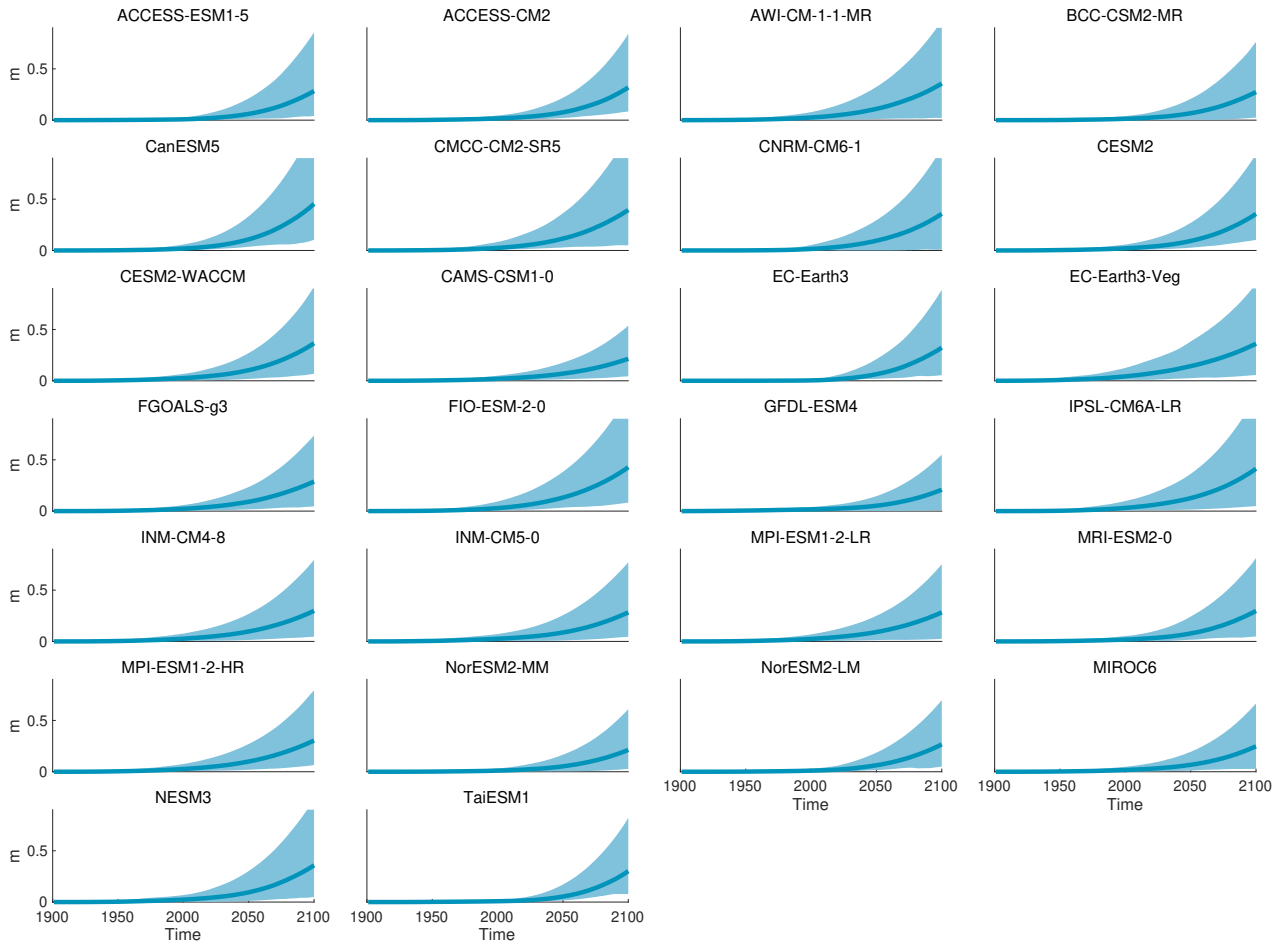
**Figure S2.** Projection of AIS dynamical SLR for each model, with shading denoting the likely range (66th percentile around the mean).

$0.0302 * x^2 + 0.8036 * x + 2.2007$
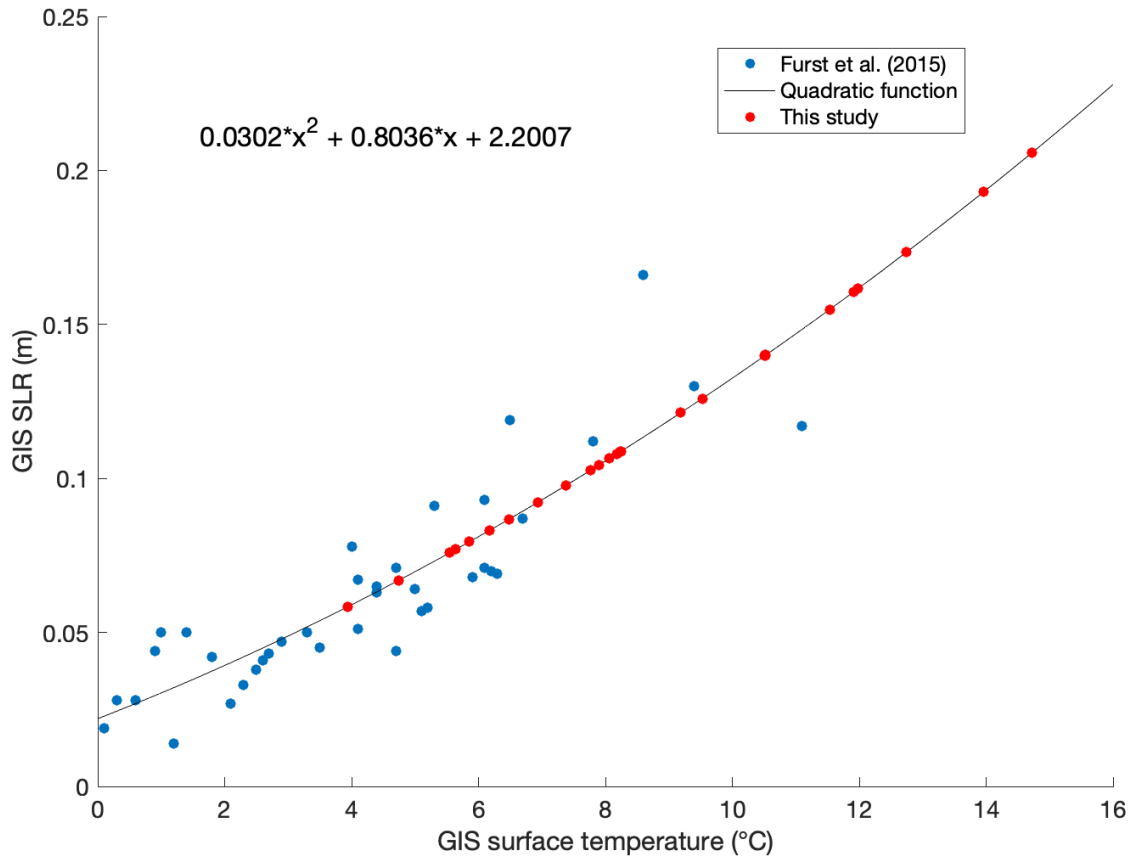
**Figure S3.** Relationship between Greenland Ice Sheet mass loss and temperature change derived from CMIP5 models in Fürst et al. (2015) (blue points). Red points show the estimates using the CMIP6 models in this study.
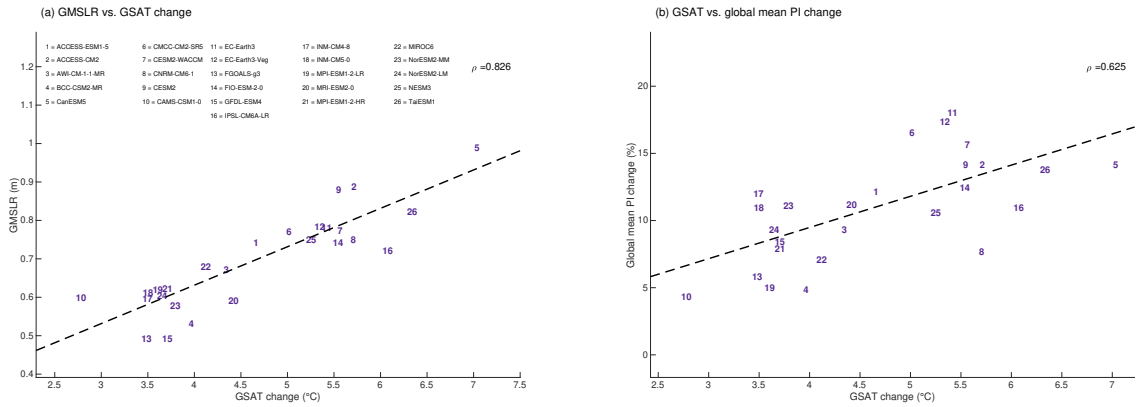
**Figure S4.** Scatter plots showing (a) global mean sea level rise and global mean temperature change and (b) global potential intensity change and global mean temperature change for each model.
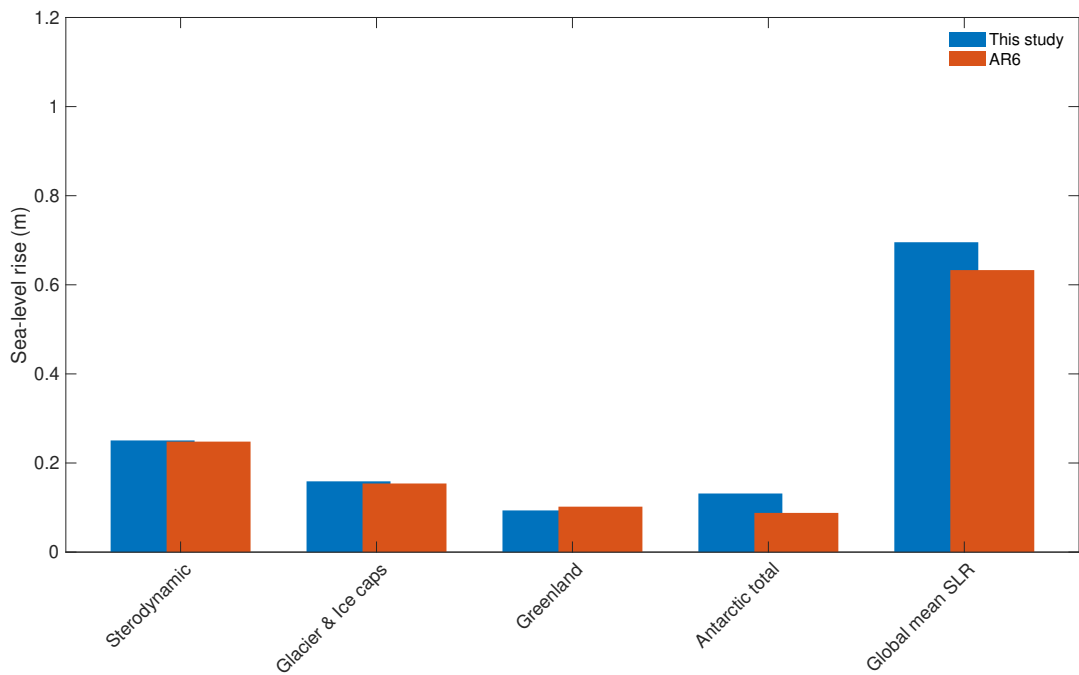


**Figure S5.** Global mean sea level rise projection comparison between AR6 and this study.
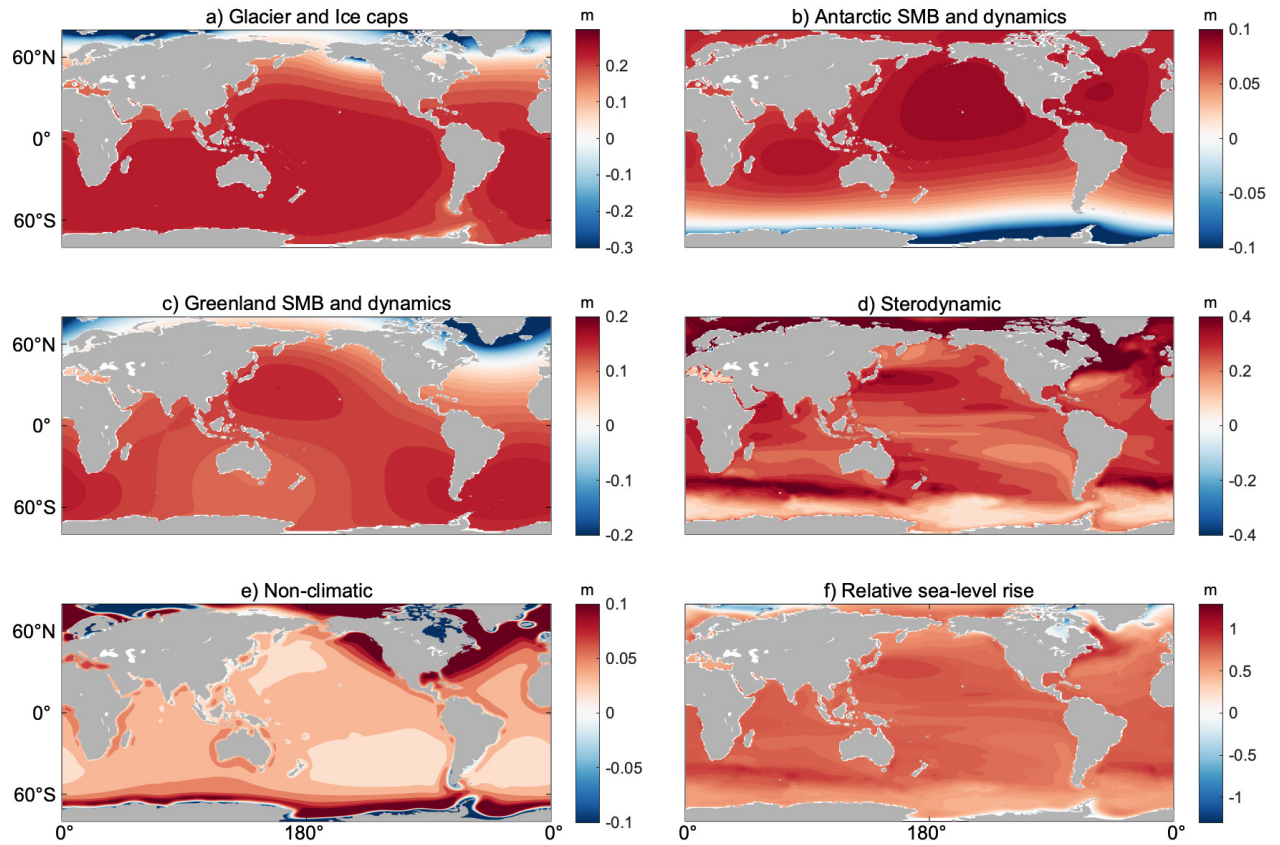
**Figure S6.** CMIP6 ensemble mean sea-level rise difference maps of (a) GIC, (b) AIS, (c) GIC, (d) sterodynamic, (e) non-climatic and (f) relative SLR for SSP5-8.5.
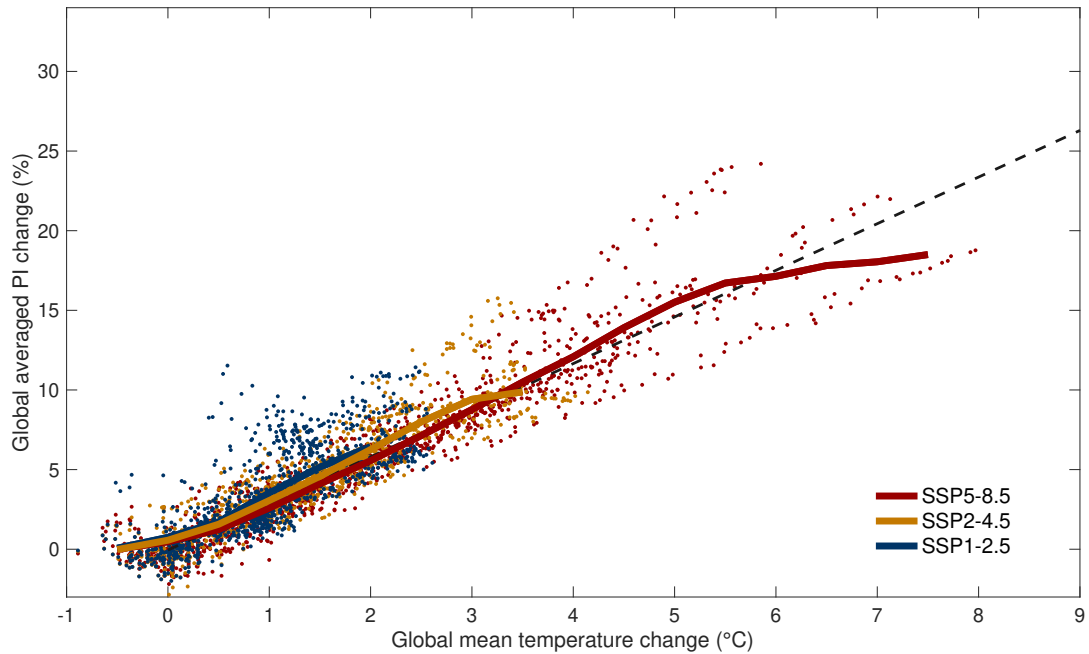
**Figure S7.** Globally averaged PI change (%) and global mean temperature change for the SSP5-8.5 (red), SSP2-4.5 (yellow) and SSP1-2.5 (blue) scenarios. Each point denotes one year for one model between years 2014 - 2100. Only eleven CMIP6 models are displayed (ACCESS-ESM1-5, ACCESS-CM2, CanESM5, CMCC-CM2-SR5, IPSL-CM6A-LR, INM-CM4-8, INM-CM5-0, MPI-ESM1-2-LR, MRI-ESM2-0, MPI-ESM1-2-HR, MIROC6). These models cover the full range of modeled ECS and GSAT temperature change (Fig. S1).
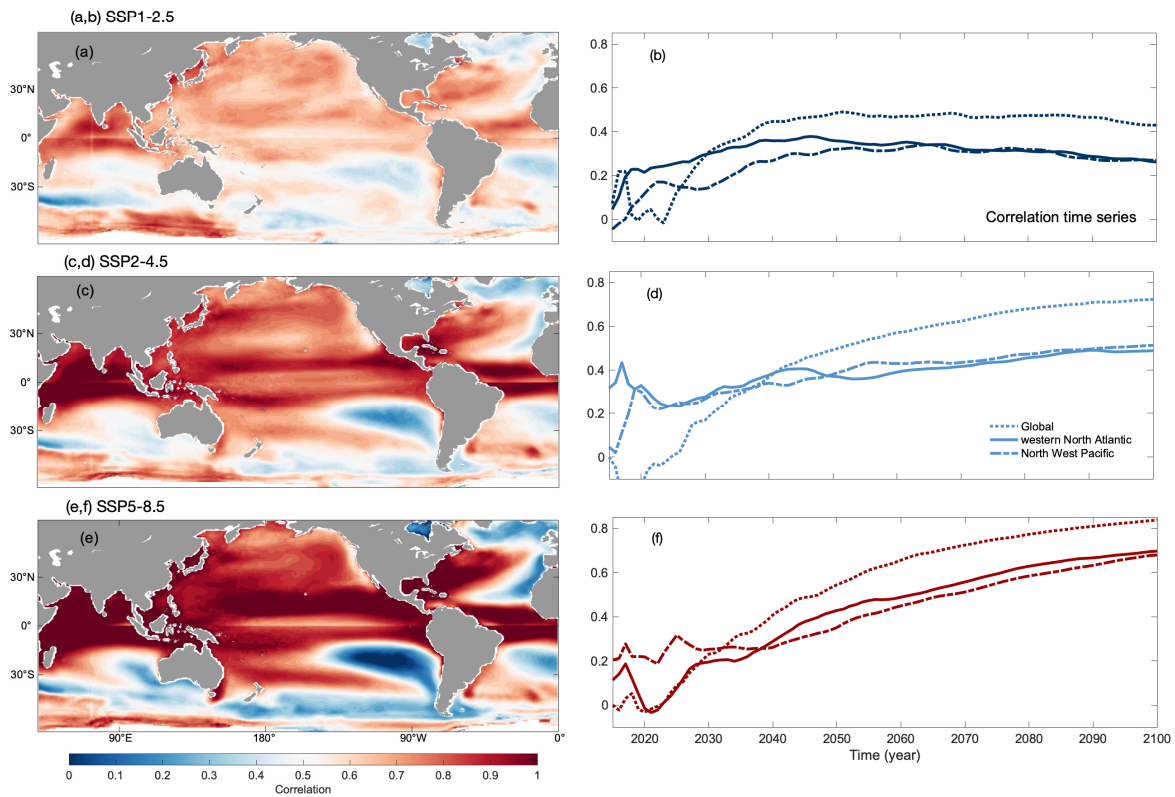
**Figure S8.** Ensemble averages of intra-model correlations between relative SLR and PI change over space (a,c,e) and time (b,d,f). For each model, correlations are calculated over the 86 years of the SSP1-2.5 (a,b), SSP2-4.5 (c,d) and SSP5-8.5 (e,f) scenarios. Averages are over eleven CMIP6 models (ACCESS-ESM1-5, ACCESS-CM2, CanESM5, CMCC-CM2-SR5, IPSL-CM6A-LR, INM-CM4-8, INM-CM5-0, MPI-ESM1-2-LR, MRI-ESM2-0, MPI-ESM1-2-HR, MIROC6). These models span the full range of modeled GSAT change (Fig. S1). Time-series of correlations (b,d,f) are calculated relative to year 2014.

PI and vertical wind shear
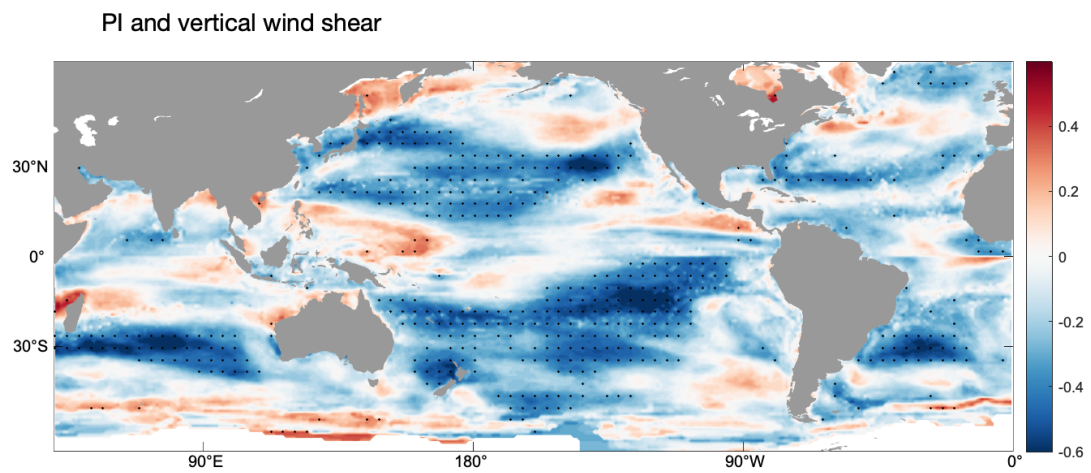


**Figure S9.** Inter-model correlation between PI and vertical wind shear. Stipples denote correlations significant to 95%.
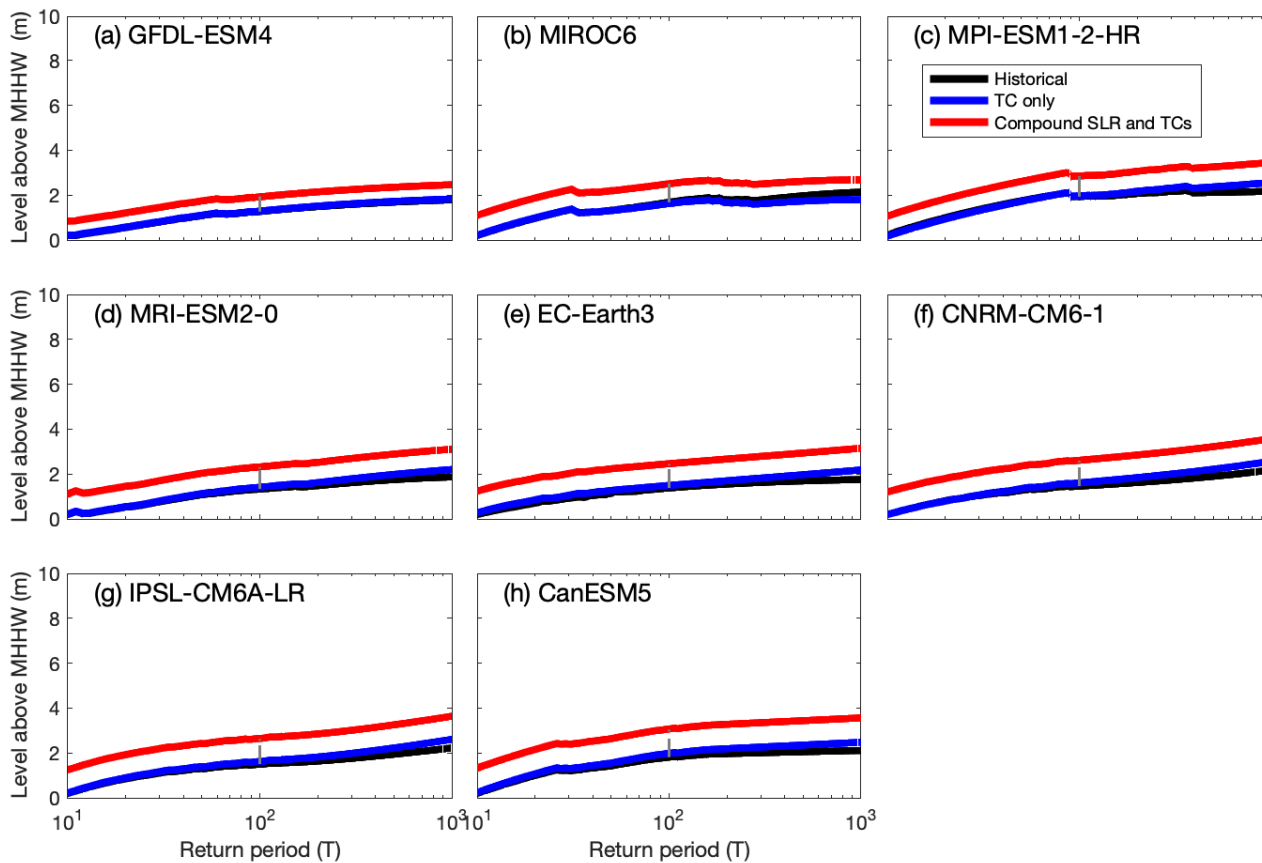
**Figure S10.** Same as Figure 4, but assuming no change in TC frequency at NYC. Estimated storm tide return levels for the historical period of 1994-2014 (black) and future period of 2080–2100 (blue: only effects of TC changes, red: compound effects of SLR and TCs) at New York City.
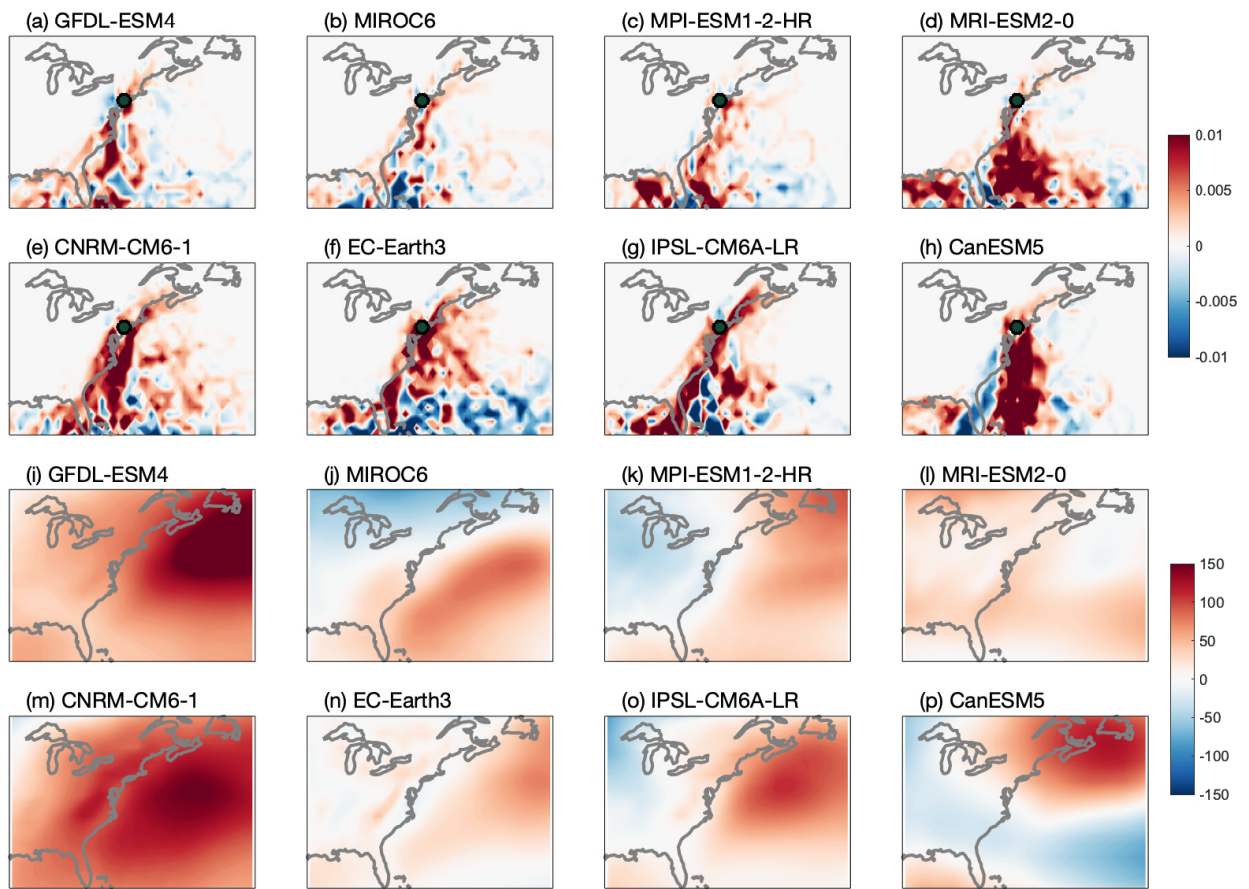
**Figure S11.** Mean difference between future and modern synthetic TC track densities for each model (a-h). Track densities are determined by the sum total of tracks crossing through each grid box over 20-year periods from 2080–2100 and 1994–2014, divided by the area of that grid box and the number of years. Also shown are the mean sea-level pressure differences (pascals) averaged over June - November for the eight CMIP6 modeled with ADCIRC (i-p).
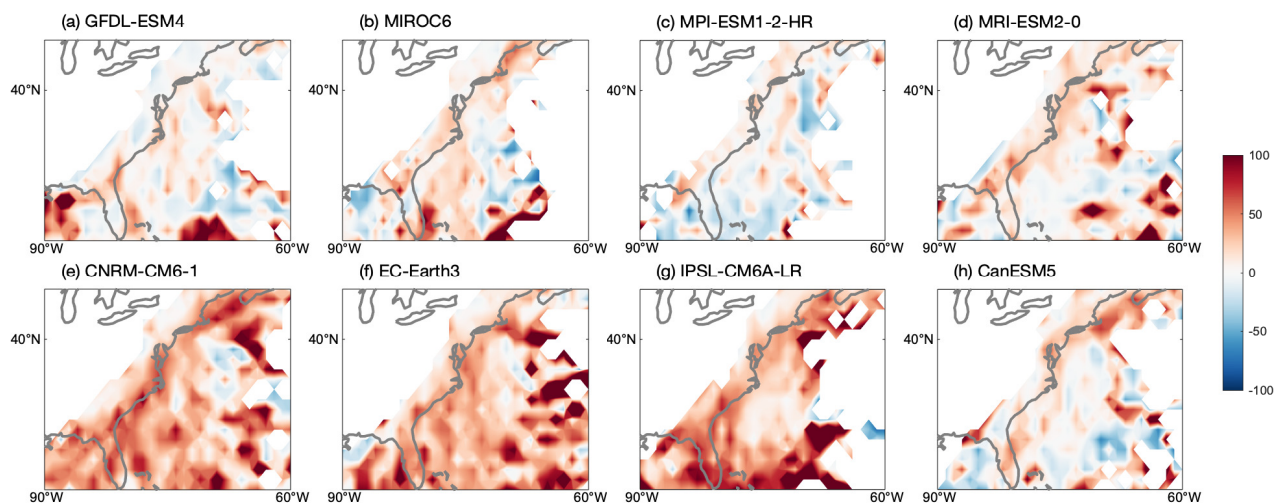
**Figure S12.** Mean projected changes in Vmax shown as percentage increases from years 1994-2014 of the historical simulation.
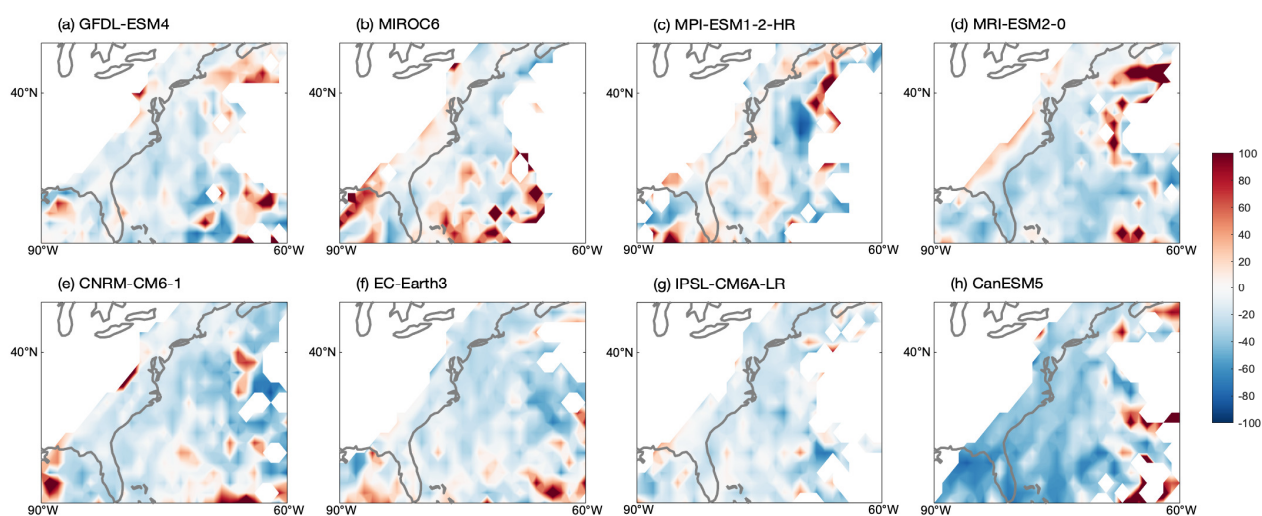


**Figure S13.** Mean projected changes in translation speed shown as percentage increases from years 1994-2014 of the historical simulation.

:
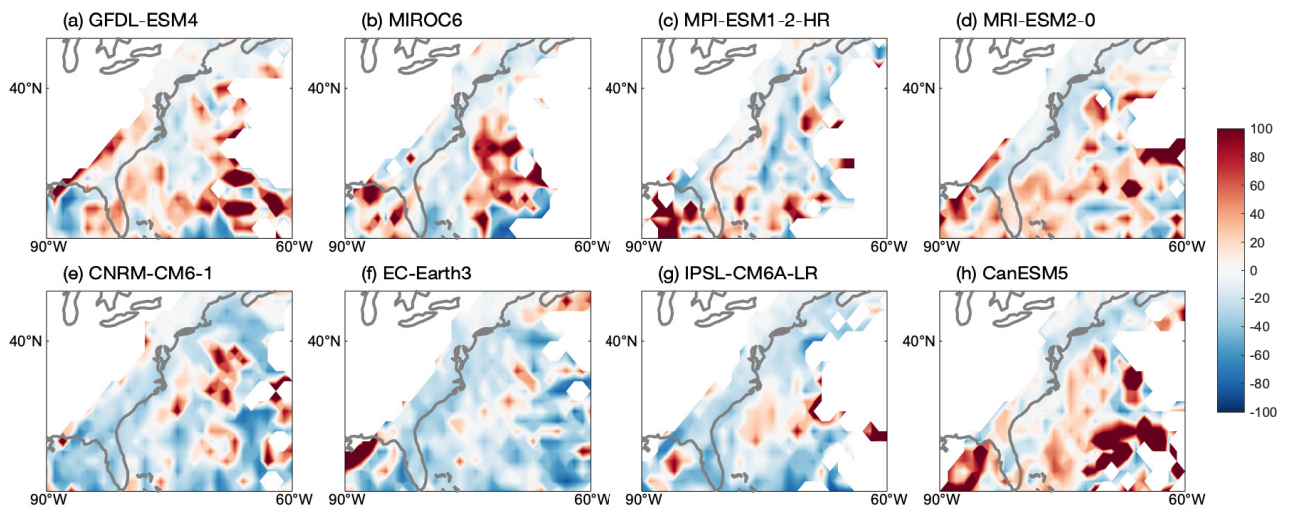


**Figure S14.** Mean projected changes in radius of maximum wind speed shown as percentage increases from years 1994-2014 of the historical simulation.

September 28, 2021, 2:53pm
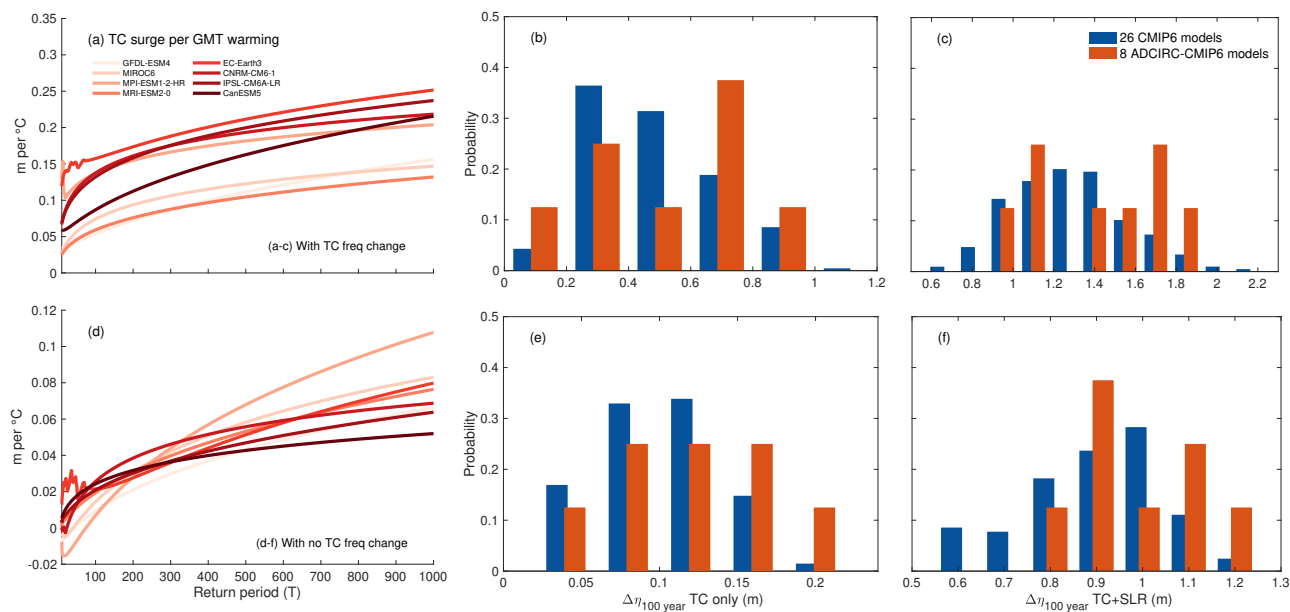
**Figure S15.** (a,d) Scaling relationships between TC surge changes at NYC and global mean temperature (GSAT) change for the eight ADCIRC-CMIP6 models, assuming change (top) and no change (bottom) in TC frequency. Probability density functions (PDF) show the change to the historical 100 year flood event ($\Delta\eta_{100}$) resulting from TC climatology change (b,e) and both SLR and TC climatology change (c,f) for the ADCIRC-CMIP6 models (red) and all 26 CMIP6 models (blue). To produce the PDFs for all 26 CMIP6 models (blue), we randomly sample one of the eight scaling factors and one of the 26 CMIP6 models GSAT and SLR projections 100,000 times.
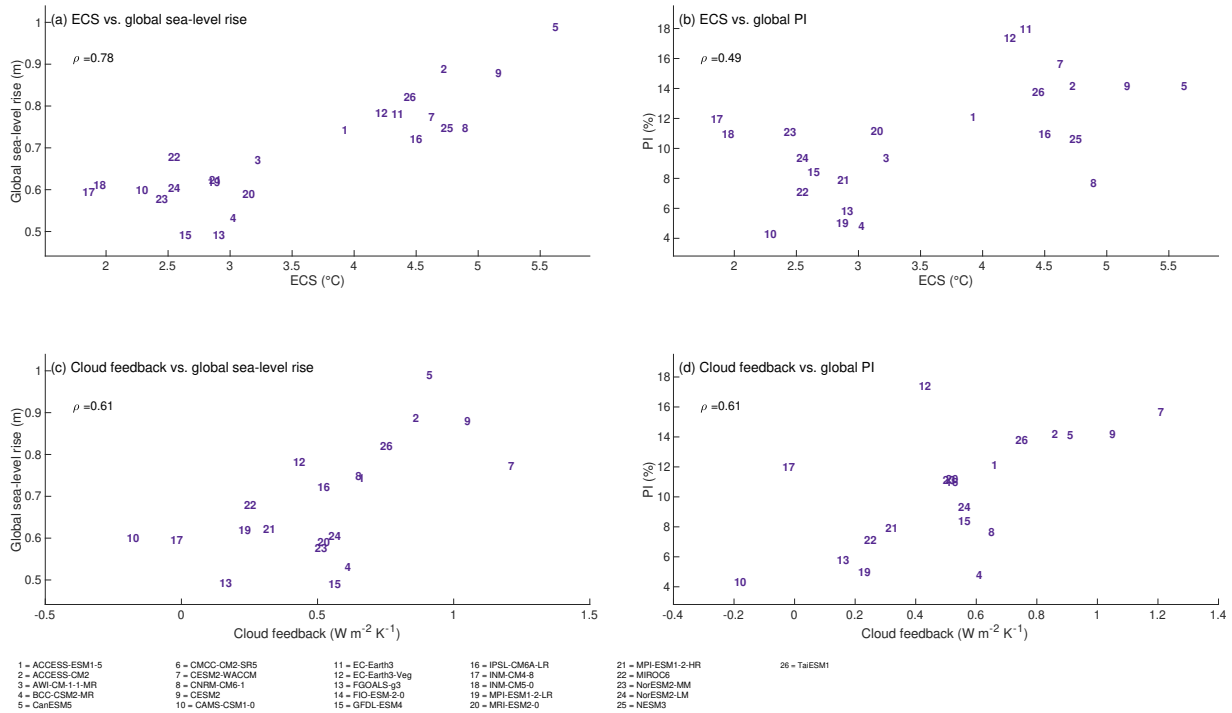
**Figure S16.** Scatter plots showing global mean sea level rise against effective climate sensitivity (ECS) (a) and cloud feedback (c). Also shown is global averaged potential intensity against ECS (b) and cloud feedback (d). Cloud feedback values are from Wang et al. (2021). ECS values are from Wang et al. (2021) and Zelinka et al. (2020).
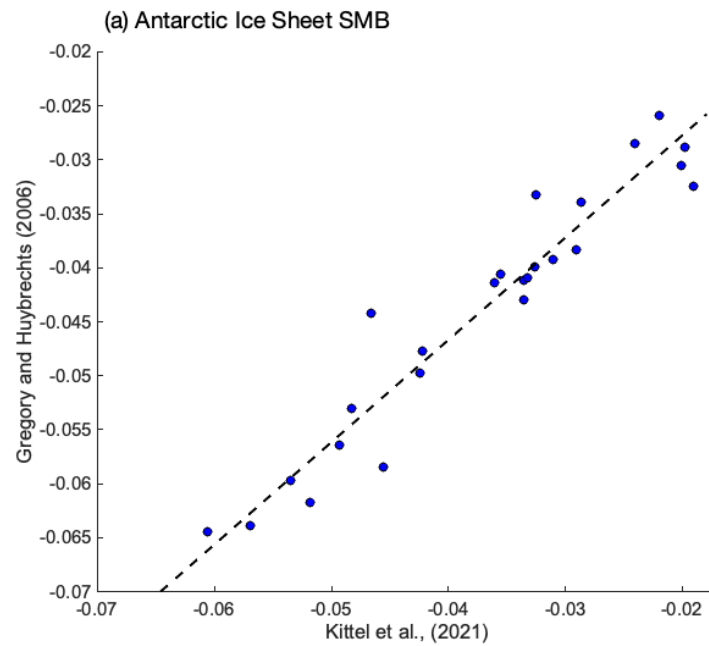
**Figure S17.** Comparison between the two methods (Gregory and Huybrechts (2006) and Kittel et al. (2021)) used to model Antarctic Ice Sheet surface mass balance changes. Each point denotes one CMIP6 model.